Finite-Time Prescribed Performance Fault-Tolerant Attitude Control for Rocket Substage Recovery by Parafoil

Xiaojun Xing, *Member, IEEE*, Wenxin Yang, Linfeng Qin, Bing Xiao, *Senior Member, IEEE*, and Feisheng Yang, *Member, IEEE*

***Abstract*—Parafoil is one of the important approaches for achieving low-cost and precise recovery of the rocket substage. To address the challenges posed by uncertain disturbances and faults such as partial failures and biases in parafoil actuators arising from the extreme multiphysics field coupling environment which involves force, thermal, electrical, and magnetic effects, as well as the strong coupling and nonlinearity inherent in the rocket substage and parafoil, a fault-tolerant attitude controller is proposed in this article, which integrates finite-time prescribed performance backstepping sliding mode control (FPBSMC) with sliding mode disturbance observer (SMDO) to effectively compensate for actuator faults and suppress uncertain lumped disturbances, ensuring stable attitude control of the parafoil-substage combination (PSC). First, the nonlinear model of the PSC and the actuator fault model are established. Second, the SMDO is proposed to estimate the lumped disturbance torque caused by uncertain disturbances and actuator faults. Third, the FPBSMC fault-tolerant attitude controller is developed to compensate for the lumped disturbance torque and achieve high-precision, rapid fault-tolerant attitude control of the PSC. Finally, numerical simulations and hardware-in-loop experiments are conducted to validate the controller's performance under various fault scenarios. The experimental results demonstrate that the proposed FPBSMC and SMDO-based controller achieves excellent fault-tolerant performance and attitude tracking accuracy, even under actuator faults and uncertain disturbances.**

***Index Terms*—Actuator faults, attitude fault-tolerant control, parafoil, rocket substage recovery.**

I. Introduction

THE accurate recovery of rocket substages plays a significant role in controlling the landing area of rocket substages, enabling their reuse, and significantly reducing the cost of rocket launches. It also ensures the safety of the landing area and facilitates low-cost, high-frequency launches required for future rocket missions. Thus, rocket substage recovery has become a research hotspot in the field of aerospace [1]. Among the available recovery methods, parafoil is an ideal solution for high-precision rocket substage recovery due to its excellent glide stability, maneuverability, low costs, and high landing accuracy.

Controllable parafoil is a lightweight aircraft, whose actuator is comprised of motors and winches. Due to flexible connection between parafoil and rocket substage, relative motion is frequently observed between them during recovery. Furthermore, as parafoil is installed at the tail section of rocket substage before launching, it is continuously exposed to an extremely complex environment, which is characterized by multiphysical fields couplings, including thermal, mechanical, electrical, and magnetic interactions, in the entire process spanning from launch through payload separation to substage reentry. Such conditions give rise to numerous uncertain disturbances, thereby imposing stringent demands on the reliability and fault-tolerant control performance of parafoil actuators. Additionally, the limited tail space of rocket substage constrains the ability to install multiple redundant parafoil actuators, shown in Fig. 1, thus it is difficult to realize fault tolerance by physical redundancy. Therefore, it is of great significant theoretical and practical value to develop a model-driven active fault-tolerant attitude controller under actuator failure scenarios.

In recent years, numerous fault-tolerant control methods have been developed to enhance the stability and dynamic performance of the plant under actuator faults and uncertain disturbances. In [2], [3], an adaptive observer was integrated into

Received 6 March 2025; revised 28 June 2025; accepted 30 July 2025. This work was supported in part by the National Natural Science Foundation of China under Grant 62573358 and Grant 62273283; in part by the Industry-University-Research Innovation Fund of Chinese Universities under Grant 2021ZYA03006; in part by the Natural Science Basic Research Program of Shaanxi under Grant 2024JC-YBMS-500; and in part by the Guangdong Basic and Applied Basic Research Foundation under Grant 2024A1515010674. *(Corresponding author: Bing Xiao.)*

Xiaojun Xing is with the Research and Development Institute of Northwestern Polytechnical University, Shenzhen 518063, China, and also with the School of Automation, Northwestern Polytechnical University, Xi'an 710129, China (e-mail: xxiaojun@nwpu.edu.cn).

Wenxin Yang, Bing Xiao, and Feisheng Yang are with the School of Automation, Northwestern Polytechnical University, Xi'an 710129, China (e-mail: 2023202528@mail.nwpu.edu.cn; xiaobing@nwpu.edu.cn; yangfeisheng@nwpu.edu.cn).

Linfeng Qin is with the Xi'an ASN Technology Group Company Ltd., Xi'an 710065, China (e-mail: qinlinfeng@mail.nwpu.edu.cn).

Digital Object Identifier 10.1109/TIE.2025.3598212

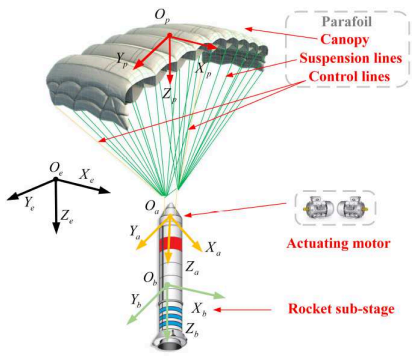

Fig. 1. Coordinate systems of PSC.

controller for launch vehicles to restrain disturbances and estimate faults. In [4], a robust fault-tolerant scheme based on adaptive backstepping nonsingular fast terminal sliding mode control was proposed for robot manipulators. In [5], based on the second-order fast nonsingular terminal sliding mode control, a novel adaptive fault-tolerant controller was developed for quadrotor. In [6], an adaptive reconfigurable active fault-tolerant control scheme was developed for multiple unmanned surface vehicles based on observer and projection law-based estimation. In [7], for the attitude of UAV, a sliding-mode-based adaptive observer is utilized to estimate the stuck fault and compensate for the estimation mismatch and unknown disturbances. In [8], [9], an active fault-tolerant control was proposed for spacecraft attitude control under actuator faults. In [10], an active fault-tolerant controller with adaptive compensation mechanism was designed for nonlinear systems by command filtering backstepping method. In [11], actuator faults were estimated and compensated using safety-constrained train position and speed data by projection algorithm. In [12], a fixed time fault-tolerant controller was designed for spacecraft by utilizing prescribed performance control (PPC) and reinforcement learning under actuator faults and external disturbances. In [13], [14], an adaptive compensation mechanism was developed for multi-UAV and spacecraft to solve actuator failures and improve fault tolerance capability. In [15], an attitude controller for flexible spacecraft was proposed by combination of PPC and barrier Lyapunov function under disturbances and actuator faults. In [16], the advantages and disadvantages of existing engineering fault-tolerant control techniques and theoretical methodologies are discussed. In [17], various theoretical and practical design approaches were critically assessed to achieve the desired level of fault-tolerance for the spacecraft's attitude control.

Nowadays, the application of fault-tolerant control in rockets, unmanned aerial vehicles, and other aircrafts is widely studied. However, although significant progress has been achieved in the research on parafoil-substage combination (PSC) [18], [19], the related research on fault-tolerant control of PSC remains relatively scarce. To ensure precise and safe recovery of PSC, more attention should be paid to the research on fault tolerant control for PSC. To address actuator faults and uncertain disturbances, an attitude fault-tolerant controller based on finite-time prescribed performance backstepping sliding mode controller (FPBSMC) and a sliding mode disturbance observer (SMDO) is proposed, which effectively mitigates the impacts of actuator faults and uncertain disturbances. The main contributions of this article are as follows.

1) To address actuator faults and uncertain disturbances in rocket substage recovery by parafoil, an actuator fault model of PSC is established, and a fault-tolerant control scheme based on FPBSMC and SMDO is proposed. SMDO is utilized to estimate the lumped disturbance torque caused by actuator faults and uncertain disturbances, while FPBSMC ensures high-precision and rapid fault-tolerant attitude control of PSC.
2) Based on finite time control theory and PPC theory, FPBSMC is developed by integration of PPC and backstepping sliding mode control (BSMC). Experimental results demonstrate that the proposed controller achieves precise attitude tracking and exhibits strong fault-tolerant performance under actuator faults and uncertain disturbances.

The remainder of this article is organized as follows: Section II presents the dynamics model of PSC and the modeling of actuator faults. Section III details the framework and design procedure of the SMDO and FPBSMC. Simulation and hardware-in-loop experimental results are provided in Section IV. Finally, Section V summarizes the study and outlines future research perspectives.

II. Modeling

In this section, the kinematics and dynamics model of PSC is established under normal operational conditions. On this basis, the typical fault model of parafoil actuator is built and introduced into the normal model of PSC.

A. Model of PSC

PSC model incorporates four coordinate systems including geodetic coordinate system Ω_e, parafoil body coordinate system Ω_p, rocket substage coordinate system Ω_b, and airflow coordinate system Ω_a, which are shown in Fig. 1. The transformation matrices between these coordinate systems are defined as $\mathbf{T}_{p-e}$ which is from Ω_e to Ω_p, $\mathbf{T}_{b-e}$ which is from Ω_e to Ω_b, and $\mathbf{T}_{a-p}$ which is from Ω_p to Ω_a. Detailed expressions can be found in our previous work [19].

The dynamic model of PSC is

$$\begin{bmatrix} \dot{\mathbf{w}}_p^{\mathrm{T}} \\ \dot{\mathbf{w}}_b^{\mathrm{T}} \\ \dot{\mathbf{V}}_c^{\mathrm{T}} \\ \dot{\mathbf{F}}_r^{\mathrm{T}} \end{bmatrix} = \left(\mathbf{A}^{\mathrm{T}}\right)^{-1} \begin{bmatrix} \mathbf{B}_1 \\ \mathbf{B}_2 \\ \mathbf{B}_3 \\ \mathbf{B}_4 \end{bmatrix} \tag{1}$$

where $\mathbf{A}$ and $\mathbf{B}_i$ are

$$\mathbf{A} = \begin{bmatrix} \mathbf{0}_{3\times3} & \mathbf{I}_p + \mathbf{I}_{af} & \mathbf{0}_{3\times3} & \mathbf{R}_{cp}^{\times}\mathbf{T}_{p-e} \\ m_b\mathbf{T}_{b-e} & \mathbf{0}_{3\times3} & -m_b\mathbf{R}_{cb}^{\times} & \mathbf{T}_{b-e} \\ \left(m_p\mathbf{I}_{3\times3} + \mathbf{M}_{af}\right)\mathbf{T}_{p-e} & -\left(m_p\mathbf{I}_{3\times3} + \mathbf{M}_{af}\right)\mathbf{R}_{cp}^{\times} & \mathbf{0}_{3\times3} & -\mathbf{T}_{p-e} \\ \mathbf{0}_{3\times3} & \mathbf{0}_{3\times3} & \mathbf{I}_b & -\mathbf{R}_{cb}^{\times}\mathbf{T}_{b-e} \end{bmatrix}$$

$$\begin{cases} \mathbf{B}_1 = \boldsymbol{\tau} - \mathbf{w}_p^{\times}\left(\mathbf{I}_p + \mathbf{I}_{af}\right)\mathbf{w}_p - \mathbf{T}_{p-e}\mathbf{T}_{b-e}^{\mathrm{T}}\mathbf{M}_c \\ \mathbf{B}_2 = \mathbf{F}_b^{\mathrm{aero}} + \mathbf{F}_b^{G} - m_b\mathbf{w}_b^{\times}\mathbf{w}_b^{\times}\mathbf{R}_{cb} \\ \mathbf{B}_3 = \mathbf{F}_p^{\mathrm{aero}} - \left(m_p\mathbf{I}_3 + \mathbf{M}_{af}\right)\mathbf{w}_p^{\times}\mathbf{w}_p^{\times}\mathbf{R}_{cp} \\ \qquad +\mathbf{F}_p^{G} - \mathbf{w}_p^{\times}\mathbf{M}_{af}\left(\mathbf{T}_{p-e}\mathbf{V}_c + \mathbf{w}_p^{\times}\mathbf{R}_{cp}\right) \\ \mathbf{B}_4 = \mathbf{M}_c - \mathbf{w}_b^{\times}\mathbf{I}_b\mathbf{w}_b - \dot{\mathbf{I}}_b^{\mathrm{var}}\mathbf{w}_b \end{cases} \tag{2}$$

where $\mathbf{0}_{3\times3}$ is zero matrix and $\mathbf{I}_{3\times3}$ is unit matrix; $\mathbf{w}_p$ represents attitude angular velocity of parafoil, $\mathbf{w}_b$ denotes attitude angular velocity of rocket substage, $\mathbf{w}_p^{\times}$ and $\mathbf{w}_b^{\times}$ are cross-product operators; $\mathbf{V}_c$ indicates velocity at the point of intersection between parafoil and rocket substage; $\mathbf{F}_r$ represents reaction force at the point of intersection; m_p and m_b are masses of parafoil and rocket substage, respectively; $\mathbf{F}_p^{\mathrm{aero}}$ and $\mathbf{F}_p^{\mathrm{G}}$ denote aerodynamic and gravitational forces acting on parafoil, while $\mathbf{F}_b^{\mathrm{aero}}$ and $\mathbf{F}_b^{\mathrm{G}}$ represent aerodynamic and gravitational forces acting on rocket substage, respectively; $\boldsymbol{\tau}$ is control torque; $\mathbf{I}_p$ and $\mathbf{I}_b$ are moments of inertia for parafoil and rocket substage, respectively; $\mathbf{R}_{cp}$ and $\mathbf{R}_{cb}$ represent distance vectors from mass centers of parafoil and rocket substage to intersection point, respectively; $\mathbf{M}_{af}$ and $\mathbf{I}_{af}$ are added mass and added moment of inertia respectively, while $\mathbf{M}_{\mathrm{app}}$ and $\mathbf{F}_{\mathrm{app}}$ are added mass force and added mass moment respectively; $\mathbf{M}_c$ denotes torsional moment; $\mathbf{I}_b^{\mathrm{var}}$ denotes unknown time-varying variable. Detailed descriptions of these parameters and their calculation equations can be found in [19].

To facilitate the effect analysis of actuator faults and uncertain disturbances, by extracting the first term of (1), the following simplified second-order model of the system can be obtained:

$$\begin{cases} \dot{\boldsymbol{\Theta}}_p = \mathbf{w}_p \\ \dot{\mathbf{w}}_p = \mathbf{I}_p^{-1}\left(-\mathbf{w}_p^{\times}\mathbf{I}_p\mathbf{w}_p + \boldsymbol{\tau} + \boldsymbol{\tau}_d\right) \end{cases} \tag{3}$$

where $\boldsymbol{\Theta}_p$ denotes attitude angle of parafoil; $\boldsymbol{\tau}_d$ represents uncertain disturbances, which include external environment disturbances, relative motion disturbances between parafoil and rocket substage, model uncertainties and so on. Refer to part A of Section IV for the similarity between the second-order model and the 9 DOF model.

B. PSC Model With Actuator Faults

The actuator of PSC consists of digital servos and operating levers. Specifically, digital servo drives operating levers, which in turn adjust tension of parafoil ropes to control the attitude and trajectory of PSC. The internal structure of digital servo consists of several key components, including controller, driver, brushless dc motor, decelerator, and feedback potentiometer. The basic control structure of actuator is shown in Fig. 2.

Where u_d denotes control command signal, u_f is feedback signal obtained by feedback potentiometer through converting ϖ, which is angular displacement of servo output.

The primary component of digital servo is a brushless dc motor, whose stator is equipped with three-phase windings. The controller continuously adjusts energized phases and current magnitudes to generate a reactive magnetic field, which is perpendicular to the rotor's magnetic field. Finally, the generated

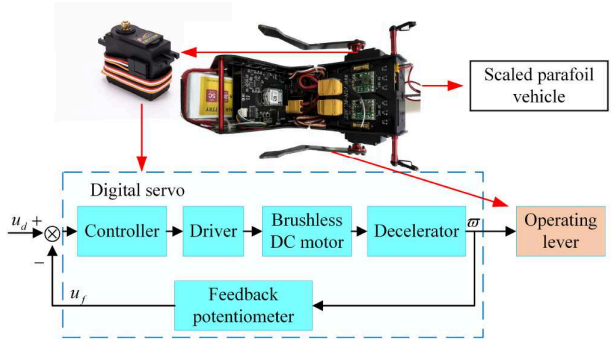

Fig. 2. Actuator of PSC.

torque is transferred to operating levers, which pull parafoil ropes to control attitude and trajectory of PSC. The energy transfer equation is expressed and the torque balance equation is described as follows:

$$e_a i_a + e_b i_b + e_c i_c = \mathbf{T}_e\boldsymbol{\Omega} \tag{4}$$

$$\mathbf{T}_e - \mathbf{T}_L = \mathbf{J}\frac{d\boldsymbol{\Omega}}{dt} + B_v\boldsymbol{\Omega} \tag{5}$$

where e_a, e_b, and e_c are back electromotive forces of three-phase windings; i_a, i_b, and i_c are three-phase currents; $\mathbf{T}_e$ represents electromagnetic torque of brushless dc motor, $\mathbf{T}_L$ denotes load torque, $\mathbf{J}$ denotes inertia torque of rotor; $\boldsymbol{\Omega}$ and B_v denote mechanical angular velocity of motor and viscous friction coefficient, respectively.

In a high-temperature environment, the thermo-resistive effect fault of the motor windings can lead to partial failure of the PSC actuator. In a complex magnetic field, magnetic bias fault of the motor can excite the actuator bias and lead to the actuator output deviating beyond the expected control command. Both faults can be modeled as

$$\boldsymbol{\tau}_c = \eta\cdot\boldsymbol{\tau} + \mathbf{T'}_e \tag{6}$$

$$\eta = \frac{\mathbf{T}_{er}}{\mathbf{T}_{ed}} \tag{7}$$

where $\boldsymbol{\tau}_c$ denotes actual control torque input to system, $\boldsymbol{\tau}$ is control torque same as that in (1), $\mathbf{T}_{ed}$ is desired torque, $\mathbf{T}_{er}$ is actual torque of brushless dc motor; η denotes the winding thermo-resistive effect fault coefficient, which represents partial failure of actuator; $\mathbf{T'}_e$ indicates magnetic bias fault, which represents additional control torque is executed by actuator as a result of the external magnetic field. Different values of two faults form the following fault scenarios.

1) $\eta = 1, \mathbf{T'}_e \neq 0$. It indicates that the magnetic bias fault of the PSC actuator, namely additive failure, occurs which will cause the attitude and trajectory of the PSC deviates.
2) $0 < \eta < 1, \mathbf{T'}_e = 0$. It means that the winding thermo-resistive effect fault of the parafoil actuator, namely multiplicative fault, occurs which will lead to partial failure and control efficiency reduction of the actuator, even large time delay in PSC attitude regulation.

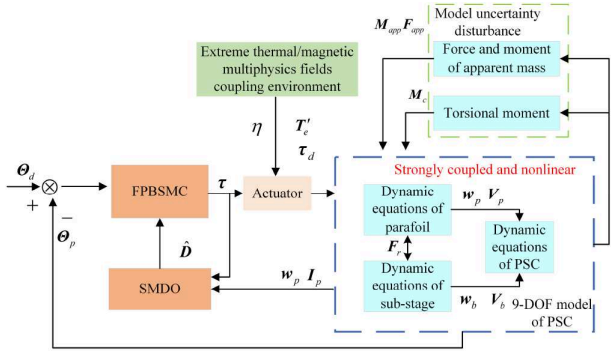

Fig. 3. Structure diagram of FPBSMC with SMDO.

3) $0 < \eta < 1, \mathbf{T'}_e \neq 0$. It shows that both winding thermo-resistive effect fault and magnetic bias fault occur simultaneously which may evoke tilt, rotation, or accidental subduction of the PSC, even rope breakage and canopy damage of the parafoil due to excessive stress accumulation.
4) $\eta = 0, \mathbf{T'}_e \neq 0$. It demonstrates that the PSC actuator is stuck, where no matter how much the control command is, the actuator always outputs $\mathbf{T'}_e$ resulting in yaw or tilt of the PSC, and failure to correct the attitude and trajectory.

In this article, we focus on the mixed faults of winding thermo-resistive effect fault and magnetic bias fault. The PSC model with actuator faults used in subsequent fault-tolerant control is as follows:

$$\begin{cases} \dot{\boldsymbol{\Theta}}_p = \mathbf{w}_p \\ \dot{\mathbf{w}}_p = \mathbf{I}_p^{-1}\left(-\mathbf{w}_p^{\times}\mathbf{I}_p\mathbf{w}_p + \boldsymbol{\tau}_c + \boldsymbol{\tau}_d\right). \end{cases} \tag{8}$$

III. FPBSMC Attitude Fault-Tolerant Controller With SMDO

The PSC FPBSMC attitude fault-tolerant controller with SMDO, listed in Fig. 3, is capable of rapidly and precisely converging to desired attitude when actuator faults occur. It can be seen that FPBSMC consists of PPC and BSMC where BSMC offers robust disturbance rejection capability and global stability, making it well-suited for highly nonlinear and strongly coupled attitude control issues in PSC. PPC can clearly set the dynamic and steady-state performance (such as overshoot, error convergence rate, and steady-state error) of the system response, ensuring that the convergence time, overshoot, and convergence accuracy are within the predefined envelope range. In this article, error convergence rate, accuracy and time are defined through a finite time prescribed performance function to quickly track desired attitude angle while enhancing accuracy and robustness of attitude control. Additionally, SMDO is proposed to estimate the lumped disturbance torque caused by actuator faults and uncertain disturbances, which is fed back to FPBSMC to compensate for the unexpected torque. The synergistic interaction between FPBSMC and SMDO significantly improves fault-tolerant capability under actuator faults and uncertain disturbances.

A. SMDO

For convenience, let $\mathbf{x}_1 = \boldsymbol{\Theta}_p$, $\mathbf{x}_2 = \mathbf{w}_p$, then (8) is transformed into a second-order state equation as follows:

$$\begin{cases} \dot{\mathbf{x}}_1 = \mathbf{x}_2 \\ \dot{\mathbf{x}}_2 = \mathbf{I}_{\mathrm{p}}{}^{-1}(-\mathbf{x}_2{}^{\times}\mathbf{I}_{\mathrm{p}}\mathbf{x}_2 + \boldsymbol{\tau}) + \mathbf{I}_{\mathrm{p}}{}^{-1}\mathbf{D} \\ \mathbf{y} = \mathbf{x}_1 \end{cases} \tag{9}$$

$$\mathbf{D} = (\eta - 1)\cdot\boldsymbol{\tau} + \mathbf{T'}_e + \boldsymbol{\tau}_d \tag{10}$$

where $\mathbf{D}$ is lumped disturbance torque of actuator faults and uncertain disturbances, assuming that $\left\|\dot{\mathbf{D}}\right\| \leq \dot{\mathbf{D}}_{\max}$ [20].

Theorem 1: For system (9) and (10), the nonsingular fast terminal sliding mode surface defined as (11) can converge in finite time

$$s = \alpha x + \dot{x} + \beta \mathrm{sig}^{p/q}(x) \tag{11}$$

where $\mathrm{sig}^{(p/q)}(x) = |x|^{(p/q)}\mathrm{sign}(x)$, $\alpha, \beta > 0$, p, q are positive odd numbers and $1 < p/q < 2$.

Proof: Let $s = 0$, (11) can be transformed into (12)

$$dt = -\frac{dx}{\alpha x + \beta \mathrm{sig}^{p/q}(x)}. \tag{12}$$

Simultaneously integrating both sides of (12), then the following result is obtained:

$$\int_0^t dt = \int_{x(0)}^{0} -\frac{dx}{\alpha x + \beta \mathrm{sig}^{p/q}(x)}. \tag{13}$$

And

$$t_s = \frac{q}{\beta(p-q)} \ln \frac{\beta x(0)^{(q-p)/p} + \alpha}{\alpha}. \tag{14}$$

Therefore, the sliding mode surface can converge to steady state in finite time t_s [21].

For (9), define the auxiliary variable $\boldsymbol{\delta}$ and the error $\mathbf{e}$.

$$\mathbf{e} = \boldsymbol{\delta} - \mathbf{x}_2. \tag{15}$$

According to Theorem 1, define the following nonsingular fast terminal sliding mode surface:

$$\mathbf{s} = \alpha_1 \mathbf{e} + \dot{\mathbf{e}} + \beta_1 \mathrm{sig}^{p_1/q_1}(\mathbf{e}). \tag{16}$$

Let the approaching law be

$$\dot{\mathbf{s}}_1 = -m\mathbf{s} - \mathrm{nsign}(\mathbf{s}) \tag{17}$$

where $m, n > 0$.

The derivative of (15) is

$$\dot{\mathbf{e}} = \dot{\boldsymbol{\delta}} - \dot{\mathbf{x}}_2. \tag{18}$$

According to (9), (16), and (18), the derivative of $\boldsymbol{\delta}$ is

$$\dot{\boldsymbol{\delta}} = \mathbf{I}_{\mathrm{p}}{}^{-1}(-\mathbf{x}_2{}^{\times}\mathbf{I}_{\mathrm{p}}\mathbf{x}_2 + \boldsymbol{\tau}) - \alpha_1\mathbf{e} - \beta_1 \mathrm{sig}^{p_1/q_1}(\mathbf{e}) + \mathbf{s}_1. \tag{19}$$

Then, the observation of disturbance torque is

$$\hat{\mathbf{D}} = \mathbf{I}_p \mathbf{s}_1. \tag{20}$$

Proof of Stability: Define the Lyapunov function V as

$$V = \frac{1}{2}\mathbf{s}^T\mathbf{s}. \tag{21}$$

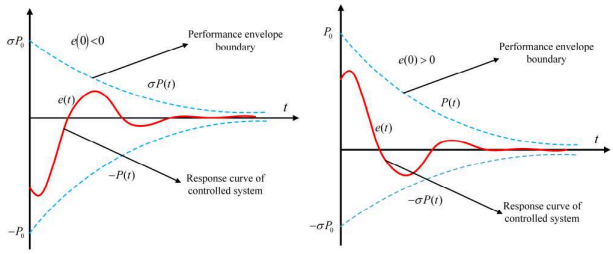

Fig. 4. PPC boundaries diagram.

The derivative of V is

$$\dot{V} = \mathbf{s}^T \dot{\mathbf{s}}. \tag{22}$$

According to (19) and (20), we can obtain

$$\dot{\mathbf{s}} = \dot{\mathbf{s}}_1 - {\mathbf{I}_\mathrm{p}}^{-1}\dot{\mathbf{D}} = -m\mathbf{s} - \mathrm{nsign}(\mathbf{s}) - {\mathbf{I}_\mathrm{p}}^{-1}\dot{\mathbf{D}}. \tag{23}$$

Substitute (23) into (22), then

$$\begin{aligned}\dot{V} &= \mathbf{s}^T(-m\mathbf{s} - \mathrm{nsign}(\mathbf{s}) - {\mathbf{I}_\mathrm{p}}^{-1}\dot{\mathbf{D}}) \\ &= -m\mathbf{s}^T\mathbf{s} - n\|\mathbf{s}\| - \mathbf{s}^T{\mathbf{I}_\mathrm{p}}^{-1}\dot{\mathbf{D}} \\ &\le -m\mathbf{s}^T\mathbf{s} - (n - \dot{\mathbf{D}}_{\max}\left\|{\mathbf{I}_\mathrm{p}}^{-1}\right\|)\|\mathbf{s}\|\end{aligned} \tag{24}$$

where $\|\mathbf{s}\|$ denotes the modulus of the pair matrix. When $n \ge \dot{\mathbf{D}}_{\max}\left\|{\mathbf{I}_\mathrm{p}}^{-1}\right\|$, $\dot{V} \le 0$. According to Lyapunov stability theorem, SMDO is stable. Furthermore, it can be seen that the sliding mode surface can converge to stable state in finite time. Consequently, the proposed observer is finite-time convergence and capable of effectively estimating the lumped disturbance torque excited by actuator faults and uncertain disturbances, which provides accurate compensation for subsequent fault-tolerant controller.

B. FPBSMC Controller

1) Prescribed Performance Control: Both transient and steady-state performance of system can be constrained by PPC to guarantee that tracking error converges to a prescribed range. The performance function and error transformation are keys to PPC [22].

For $P(t)$: $\Re^+ \cup \{0\} \to \Re^+$, it can be used as performance function if the following two conditions are met.

1) When $t \ge 0$, $P(t)$ is a smooth function, always positive and monotonically decreasing.
2) $\lim_{t\to 0}P(t) = P_0$, $\lim_{t\to\infty}P(t) = P_\infty$, $P_0 > P_\infty > 0$.

With constraints of performance function, tracking error is confined within bounds, which are shown in (25) and Fig. 4.

$$\begin{cases} -\sigma P(t) < e(t) < P(t), e(0) \ge 0 \\ -P(t) < e(t) < \sigma P(t), e(0) < 0 \end{cases} \tag{25}$$

where $0 < \sigma \le 1$.

It can be seen from Fig. 4 that when $e(0) \ge 0$, the error will be limited between the upper boundary $P(t)$ and the lower boundary $-\sigma P(t)$. When $e(0) < 0$, the error will be restricted between the upper boundary $\sigma P(t)$ and the lower boundary $-P(t)$. The following performance function is generally used:

$$F(t) = \begin{cases} \left(\frac{T_f - t}{T_f}\right)^{\frac{1}{(1-v)}}(F_0 - F_{T_f}) + F_{T_f}, t \in [0, T_f) \\ F_{T_f}, t \in [T_f, \infty] \end{cases} \tag{26}$$

where F_0, $F_{T_f}(F_0 > F_{T_f} > 0)$ are initial and final values of $F(t)$, respectively; $T_f > 0$ is convergence time, and $0 < v < 1$ is a constant. Apparently, (26) is a finite-time convergence performance function other than conventional one, its convergence time can be customized to allow error converge to final value in finite time [23].

Although the performance function provides explicit inequality constraints for error, it is complex to develop a controller directly based on the constraints. To solve this problem, the original boundary constraints are usually transformed into an equivalent unconstrained form by an appropriate unconstrained mapping function. This mapping can effectively simplify controller design process while ensuring that system meets the requirements of original performance constraints.

Define $e_i' = e_i/P_i(t)$, through a smooth and strictly monotonically increasing error mapping function $T_i(\cdot)$, the transformed error can be expressed as

$$\varepsilon_i = T_i(e_i'). \tag{27}$$

The error transformation function is

$$\begin{cases} \varepsilon_i = T_i(e'_i) = \ln\left[\frac{\sigma + e'_i}{\sigma(1 - e'_i)}\right], e_{i0} \ge 0 \\ \varepsilon_i = T_i(e'_i) = \ln\left[\frac{\sigma(1 + e'_i)}{\sigma - e'_i}\right], e_{i0} < 0. \end{cases} \tag{28}$$

The transformed error ε_i and the derivative of ε_i are utilized in following controller. The derivative of ε_i is

$$\dot{\varepsilon}_i = g(\dot{e}_i - e_i h) \tag{29}$$

where

$$g = \frac{\partial T_i}{\partial e'}{P_i}^{-1}(t), h = \frac{\dot{P}_i(t)}{P_i(t)}. \tag{30}$$

2) FPBSMC Controller: Define attitude tracking error as

$$\mathbf{e}_1 = \mathbf{x}_1 - \mathbf{x}_{1d} \tag{31}$$

where $\mathbf{x}_1$ is the actual attitude of parafoil, $\mathbf{x}_{1d}$ is the desired attitude of parafoil. $\boldsymbol{\varepsilon}_1$ is defined as the transformed error of $\mathbf{e}_1$. From (27)–(30), we can get

$$\boldsymbol{\varepsilon}_1 = T_i\left(\frac{\mathbf{e}_1}{F(t)}\right) \tag{32}$$

$$\dot{\boldsymbol{\varepsilon}}_1 = \boldsymbol{\kappa}(\dot{\mathbf{e}}_1 - \mathbf{e}_1\gamma) \tag{33}$$

$$\boldsymbol{\kappa} = \frac{\partial T_i}{\partial(\mathbf{e}_1/F(t))}F^{-1}(t), \gamma = \frac{\dot{F}(t)}{F(t)}. \tag{34}$$

Define the Lyapunov function V_1 as

$$V_1 = \frac{1}{2}{\boldsymbol{\varepsilon}_1}^T\boldsymbol{\varepsilon}_1. \tag{35}$$

Define a virtual control volume $\boldsymbol{\varepsilon}_2$ as

$$\boldsymbol{\varepsilon}_2 = c\boldsymbol{\varepsilon}_1 + \dot{\boldsymbol{\varepsilon}}_1 \tag{36}$$

where c is a positive constant, $\boldsymbol{\varepsilon}_2$ and $\boldsymbol{\varepsilon}_1$ are matrices with three rows and one column. The derivatives of V_1 and $\boldsymbol{\varepsilon}_2$ are

as follows:

$$\dot{V}_1 = {\boldsymbol{\varepsilon}_1}^T \dot{\boldsymbol{\varepsilon}}_1 = {\boldsymbol{\varepsilon}_1}^T(\boldsymbol{\varepsilon}_2 - c\boldsymbol{\varepsilon}_1) = -c{\boldsymbol{\varepsilon}_1}^T\boldsymbol{\varepsilon}_1 + {\boldsymbol{\varepsilon}_1}^T\boldsymbol{\varepsilon}_2 \tag{37}$$

$$\begin{aligned}\dot{\boldsymbol{\varepsilon}}_2 &= c\dot{\boldsymbol{\varepsilon}}_1 + \ddot{\boldsymbol{\varepsilon}}_1 = c\dot{\boldsymbol{\varepsilon}}_1 + \dot{\boldsymbol{\kappa}}\dot{\mathbf{e}}_1 + \boldsymbol{\kappa}\ddot{\mathbf{e}}_1 - \dot{\boldsymbol{\kappa}}\mathbf{e}_1\gamma - \boldsymbol{\kappa}\dot{\mathbf{e}}_1\gamma - \boldsymbol{\kappa}\mathbf{e}_1\dot{\gamma} \\ &= c\dot{\boldsymbol{\varepsilon}}_1 + \dot{\boldsymbol{\kappa}}\dot{\mathbf{e}}_1 + \boldsymbol{\kappa}\dot{\mathbf{x}}_2 - \boldsymbol{\kappa}\ddot{\mathbf{x}}_{1d} - \dot{\boldsymbol{\kappa}}\mathbf{e}_1\gamma - \boldsymbol{\kappa}\dot{\mathbf{e}}_1\gamma - \boldsymbol{\kappa}\mathbf{e}_1\dot{\gamma}.\end{aligned} \tag{38}$$

Based on Theorem 1, the nonsingular fast terminal sliding surface is defined as

$$\mathbf{S} = \alpha_2\boldsymbol{\varepsilon}_1 + \boldsymbol{\varepsilon}_2 + \beta_2 \mathrm{sig}^{p_2/q_2}(\boldsymbol{\varepsilon}_1). \tag{39}$$

The derivative of (39) is

$$\dot{\mathbf{S}} = \alpha_2\dot{\boldsymbol{\varepsilon}}_1 + \dot{\boldsymbol{\varepsilon}}_2 + \beta_2\frac{p_2}{q_2}|\boldsymbol{\varepsilon}_1|^{(p_2/q_2-1)}\dot{\boldsymbol{\varepsilon}}_1. \tag{40}$$

Combining (9) and (38), we can obtain

$$\begin{aligned}\dot{\mathbf{S}} = {} & (\alpha_2 + c)\dot{\boldsymbol{\varepsilon}}_1 + \dot{\boldsymbol{\kappa}}\dot{\mathbf{e}}_1 + \boldsymbol{\kappa}{\mathbf{I}_\mathrm{p}}^{-1}(-{\mathbf{x}_2}^\times\mathbf{I}_\mathrm{p}\mathbf{x}_2 + \boldsymbol{\tau}) \\ & + \boldsymbol{\kappa}{\mathbf{I}_\mathrm{p}}^{-1}\mathbf{D} - \boldsymbol{\kappa}\ddot{\mathbf{x}}_{1d} - \dot{\boldsymbol{\kappa}}\mathbf{e}_1\gamma - \boldsymbol{\kappa}\dot{\mathbf{e}}_1\gamma \\ & - \boldsymbol{\kappa}\mathbf{e}_1\dot{\gamma} + \beta_2\frac{p_2}{q_2}|\boldsymbol{\varepsilon}_1|^{(p_2/q_2-1)}\dot{\boldsymbol{\varepsilon}}_1.\end{aligned} \tag{41}$$

Define the Lyapunov function V_2 as

$$V_2 = V_1 + \frac{1}{2}\mathbf{S}^T\mathbf{S}. \tag{42}$$

The derivative of (42) is

$$\dot{V}_2 = \dot{V}_1 + \mathbf{S}^T\dot{\mathbf{S}}. \tag{43}$$

The approaching law is

$$\dot{\mathbf{S}}_1 = -\lambda\mathbf{S} - \mu\mathrm{sign}(\mathbf{S}) \tag{44}$$

where $\lambda, \mu > 0$. Then the FPBSMC fault-tolerant controller can be developed as

$$\begin{aligned}\boldsymbol{\tau} = {} & \mathbf{I}_\mathrm{p}\boldsymbol{\kappa}^{-1}[-(\alpha_2 + c)\dot{\boldsymbol{\varepsilon}}_1 - \dot{\boldsymbol{\kappa}}\dot{\mathbf{e}}_1 + \boldsymbol{\kappa}\ddot{\mathbf{x}}_{1d} + \dot{\boldsymbol{\kappa}}\mathbf{e}_1\gamma \\ & + \boldsymbol{\kappa}\dot{\mathbf{e}}_1\gamma + \boldsymbol{\kappa}\mathbf{e}_1\dot{\gamma} - \beta_2\frac{p_2}{q_2}|\boldsymbol{\varepsilon}_1|^{(p_2/q_2-1)}\dot{\boldsymbol{\varepsilon}}_1 \\ & - \lambda\mathbf{S} - \mu\mathrm{sign}(\mathbf{S})] + {\mathbf{x}_2}^\times\mathbf{I}_\mathrm{p}\mathbf{x}_2 - {\mathbf{I}_\mathrm{p}}^{-1}\hat{\mathbf{D}}\end{aligned} \tag{45}$$

where $\hat{\mathbf{D}}$ represents the estimation of SMDO for the disturbance torque caused by actuator faults and uncertain disturbances.

Proof of Stability: Substitute (41) and (45) into (43), yields

$$\dot{V}_2 = -c{\boldsymbol{\varepsilon}_1}^T\boldsymbol{\varepsilon}_1 + {\boldsymbol{\varepsilon}_1}^T\boldsymbol{\varepsilon}_2 - \lambda\mathbf{S}^T\mathbf{S} - \mu\left\|\mathbf{S}\right\|. \tag{46}$$

Define $\boldsymbol{\chi} = \mathrm{sig}^{p_2/q_2}(\boldsymbol{\varepsilon}_1)$.

$$\begin{aligned}\mathbf{S}^T\mathbf{S} = {} & {\alpha_2}^2{\boldsymbol{\varepsilon}_1}^T\boldsymbol{\varepsilon}_1 + \alpha_2{\boldsymbol{\varepsilon}_1}^T\boldsymbol{\varepsilon}_2 + \alpha_2\beta_2{\boldsymbol{\varepsilon}_1}^T\boldsymbol{\chi} \\ & + \alpha_2{\boldsymbol{\varepsilon}_2}^T\boldsymbol{\varepsilon}_1 + {\boldsymbol{\varepsilon}_2}^T\boldsymbol{\varepsilon}_2 + \beta_2{\boldsymbol{\varepsilon}_2}^T\boldsymbol{\chi} \\ & + \alpha_2\beta_2\boldsymbol{\chi}^T\boldsymbol{\varepsilon}_1 + \beta_2\boldsymbol{\chi}^T\boldsymbol{\varepsilon}_2 + {\beta_2}^2\boldsymbol{\chi}^T\boldsymbol{\chi}.\end{aligned} \tag{47}$$

Then

$${\boldsymbol{\varepsilon}_1}^T\boldsymbol{\varepsilon}_2 - \lambda\mathbf{S}^T\mathbf{S} = -\lambda\left(-\frac{1}{2\lambda}{\boldsymbol{\varepsilon}_1}^T\boldsymbol{\varepsilon}_2 - \frac{1}{2\lambda}\boldsymbol{\varepsilon}_1{\boldsymbol{\varepsilon}_2}^T + \mathbf{S}^T\mathbf{S}\right). \tag{48}$$

Substitute (47) into (48), then

$$\begin{aligned}&{\boldsymbol{\varepsilon}_1}^T\boldsymbol{\varepsilon}_2 - \lambda\mathbf{S}^T\mathbf{S} = -\lambda f\boldsymbol{\chi}^T\boldsymbol{\chi} \\ &-\lambda\begin{bmatrix}\boldsymbol{\varepsilon}_1 \\ \boldsymbol{\varepsilon}_2 \\ \boldsymbol{\chi}\end{bmatrix}^T\begin{bmatrix}{\alpha_2}^2 & \alpha_2 - \frac{1}{2\lambda} & \alpha_2\beta_2 \\ \alpha_2 - \frac{1}{2\lambda} & 1 & \beta_2 \\ \alpha_2\beta_2 & \beta_2 & {\beta_2}^2 - f\end{bmatrix}\begin{bmatrix}\boldsymbol{\varepsilon}_1 \\ \boldsymbol{\varepsilon}_2 \\ \boldsymbol{\chi}\end{bmatrix}.\end{aligned} \tag{49}$$

Define the following matrices:

$$\mathbf{Z} = \begin{bmatrix}\boldsymbol{\varepsilon}_1 \\ \boldsymbol{\varepsilon}_2 \\ \boldsymbol{\chi}\end{bmatrix}, Q = \begin{bmatrix}{\alpha_2}^2 & \alpha_2 - \frac{1}{2\lambda} & \alpha_2\beta_2 \\ \alpha_2 - \frac{1}{2\lambda} & 1 & \beta_2 \\ \alpha_2\beta_2 & \beta_2 & {\beta_2}^2 - f\end{bmatrix}. \tag{50}$$

Equation (46) can be rewritten as

$$\dot{V}_2 = -c{\boldsymbol{\varepsilon}_1}^T\boldsymbol{\varepsilon}_1 - \lambda f\boldsymbol{\chi}^T\boldsymbol{\chi} - \lambda\mathbf{Z}^TQ\mathbf{Z} - \mu\left\|\mathbf{S}\right\| \tag{51}$$

where $c, \lambda, \mu > 0$, $0 < f < {\beta_2}^2/2$. When Q is positive definite, $\dot{V}_2 \le 0$, then FPBSMC is stable through Lyapunov stability theorem. It can be obtained by the condition that the matrix is positive definite

$$\alpha_2 > \frac{1}{2\lambda} + 1. \tag{52}$$

When the above inequality (52) is satisfied, Q is positive definite, $\dot{V}_2 \le 0$, FPBSMC is stable. To restrain chattering, original sign function is replaced by saturation function sat in approaching law (44) while the stability is unchanging. Thus, the controller is

$$\begin{aligned}\boldsymbol{\tau} = {} & \mathbf{I}_\mathrm{p}\boldsymbol{\kappa}^{-1}[-(\alpha_2 + c)\dot{\boldsymbol{\varepsilon}}_1 - \dot{\boldsymbol{\kappa}}\dot{\mathbf{e}}_1 + \boldsymbol{\kappa}\ddot{\mathbf{x}}_{1d} + \dot{\boldsymbol{\kappa}}\mathbf{e}_1\gamma \\ & + \boldsymbol{\kappa}\dot{\mathbf{e}}_1\gamma + \boldsymbol{\kappa}\mathbf{e}_1\dot{\gamma} - \beta_2\frac{p_2}{q_2}|\boldsymbol{\varepsilon}_1|^{(p_2/q_2-1)}\dot{\boldsymbol{\varepsilon}}_1 \\ & - \lambda\mathbf{S} - \mu\mathrm{sat}(\mathbf{S})] + {\mathbf{x}_2}^\times\mathbf{I}_\mathrm{p}\mathbf{x}_2 - {\mathbf{I}_\mathrm{p}}^{-1}\hat{\mathbf{D}}.\end{aligned} \tag{53}$$

The FPBSMC attitude fault-tolerant controller is based on the nonsingular fast terminal sliding mode surface proposed in Theorem 1 to ensure that the sliding mode surface converges to a stable state in finite time. Meanwhile, the finite-time performance function is adopted to predefine the error convergence time to guarantee that the tracking error reaches the expected range in finite time. Accordingly, the FPBSMC not only is stable, but also converges in finite time, which can achieve fast and accurate tracking of the desired attitude and maintain the efficient fault-tolerant control performance under actuator faults and uncertain disturbances.

IV. Verification Experiments

In this section, the feasibility of FPBSMC attitude fault-tolerant controller with SMDO is verified by digital simulation and hardware-in-loop experiments. First, the similarity between the second-order model and the 9 DOF model is simulated, and the traditional SMC is used to simulate the fault model of PSC. Second, the performance of FPBSMC is compared with that of BSMC and prescribed performance backstepping controller (PBC) when there are no faults and SMDO. The parameters of controllers tuning experience are referred to [5]. Then, the fault-tolerant capability of FPBSMC with SMDO is evaluated. Finally, the practicality of FPBSMC with SMDO is validated through hardware-in-loop experiments.

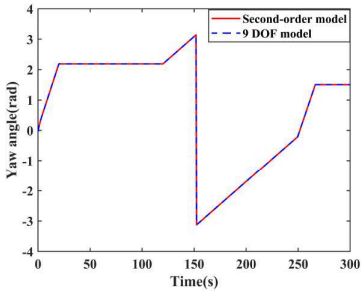

Fig. 5. Yaw angle outputs of 9 DOF model and the second-order model.

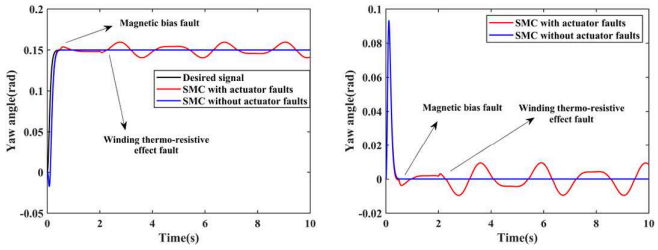

Fig. 6. Simulation results of SMC. (a) Response curve to step signal. (b) Tracking error to step signal.

A. Simulation of Model

1) Second-Order Model: The outputs of the 9 DOF model and the second-order model are compared with the same control inputs, as shown in Fig. 5. It can be seen from Fig. 5 that the yaw angle outputs of the two models remain consistent. Therefore, the simplification of the second-order model is reasonable.

2) Fault Model: An SMC illustrated in (54). Set the desired tracking signal as a step signal with a final value of 0.15rad, and a tracking differentiator (TD) [24], whose speed factor and filter factor are 20 and 5, respectively, is cascaded to smooth the step signal to avoid calculation overflow caused by derivative of step-type input. The actuator fault signals are defined as (55)

$$\begin{cases} \mathbf{e}_2 = \mathbf{x}_1 - \mathbf{x}_{1d} \\ \mathbf{s}_2 = w\mathbf{e}_2 + \dot{\mathbf{e}}_2 \\ \boldsymbol{\tau}_1 = \mathbf{I}_{\mathrm{p}}(-k\mathbf{s}_2 - k'\mathrm{sign}(\mathbf{s}_2) - w\dot{\mathbf{e}}_2 + \ddot{\mathbf{x}}_{1d}) + \mathbf{x}_2{}^{\times}\mathbf{I}_{\mathrm{p}}\mathbf{x}_2 \end{cases} \tag{54}$$

where $k, w, k' > 0$.

$$\begin{cases} \eta = 1, \mathbf{T}'_e = 0, 0s \le t < 0.5s \\ \eta = 1, \mathbf{T}'_e = 50000\sin(3t - 0.02), t \ge 0.5s \\ \eta = 0.5, \mathbf{T}'_e = 50000\sin(3t - 0.02), t \ge 2s. \end{cases} \tag{55}$$

The parameters of SMC are set as $k = 30, w = 50, k' = 1$. The simulation results are shown in Fig. 6. It can be found that SMC fails to track the desired attitude angle precisely and effectively, and tracking error changes abruptly when actuator fault occurs.

B. Simulation of FPBSMC

The desired signal is set as a sinusoidal signal whose amplitude, frequency, and initial value are 0.2rad, 1rad/s, –0.15rad,

TABLE I
CONTROLLERS PARAMETERS WITHOUT SMDO AND FAULT

Parameter	Value	Parameter	Value	Parameter	Value
k_1	0.8	k_2	50	k_3	5
k_4	8	k_5	12	ρ_0	0.1 rad
l_1	50	l_2	1	ρ_∞	0.002 rad
σ	1	c	2	α_2	60
β_2	40	p_2	13	q_2	9
λ	60	μ	10	P_0	0.1 rad
P_{T_f}	0.002 rad	T_f	1.5s	v	0.45

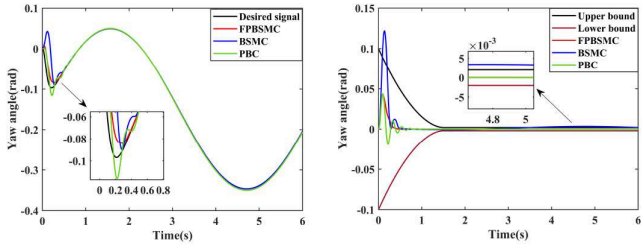

Fig. 7. Simulation results without faults and SMDO. (a) Response curves to desired signal. (b) Tracking errors to desired signal.

respectively. A BSMC illustrated in (56). A PBC listed in (57) for PSC with faults are also proposed

$$\begin{cases} \mathbf{e}_3 = \mathbf{x}_1 - \mathbf{x}_{1d} \\ \mathbf{x}_{2d} = -k_1\mathbf{e}_3 + \dot{\mathbf{x}}_{1d} \\ \mathbf{e'}_3 = \mathbf{x}_2 - \mathbf{x}_{2d} \\ \mathbf{s}_3 = l_1\mathbf{e}_3 + \mathbf{e'}_3 \\ \boldsymbol{\tau}_2 = \mathbf{I}_{\mathrm{p}}(-k_2\mathbf{s}_3 - k_3\mathrm{sign}(\mathbf{s}_3) - (k_1 + l_1)\dot{\mathbf{e}}_3 \\ \qquad +\ddot{\mathbf{x}}_{1d} - \mathbf{e}_3) + \mathbf{x}_2{}^{\times}\mathbf{I}_{\mathrm{p}}\mathbf{x}_2 \end{cases} \tag{56}$$

$$\begin{cases} \rho(t) = (\rho_0 - \rho_\infty)\exp(-l_2 t) + \rho_\infty \\ \mathbf{e}_4 = \mathbf{x}_1 - \mathbf{x}_{1d} \\ \mathbf{x}_{2d} = \mathbf{e}_4\boldsymbol{\kappa}' - k_4\gamma'^{-1}\boldsymbol{\varepsilon}' + \dot{\mathbf{x}}_{1d} \\ \mathbf{e'}_4 = \mathbf{x}_2 - \mathbf{x}_{2d} \\ \boldsymbol{\tau}_3 = -\mathbf{I}_{\mathbf{p}}\gamma'^{T}\boldsymbol{\varepsilon}' - k_5\mathbf{I}_{\mathbf{p}}\mathbf{e'}_4 + \mathbf{I}_{\mathbf{p}}\dot{\mathbf{x}}_{2d} + \mathbf{x}_2^{\times}\mathbf{I}_p\mathbf{x}_2 \end{cases} \tag{57}$$

where $\mathbf{x}_{2d}$ are virtual control quantities. $\rho(t)$ is a prescribed performance function. $\boldsymbol{\varepsilon}'$ is transformed error and $\boldsymbol{\kappa}', \gamma'$ can refer to (34). $k_1, k_2, k_3, k_3, k_4, k_5, l_1, l_2, \rho_0, \rho_\infty$ are positive constants.

1) Control Performance: The parameters of controllers without SMDO and actuator faults are listed in Table I.

The simulation results presented in Fig. 7 demonstrate that the three controllers successfully track the desired signal; however, FPBSMC demonstrates better tracking performance. It can be seen from Fig. 7(b) that compared with the BSMC and PBC, the FPBSMC converges faster in finite time. The tracking error is well limited within the prescribed boundary, and the final error is smaller.

2) Fault-Tolerant Performance: The fault-tolerant performance of the FPBSMC with or without SMDO, is compared with BSMC and PBC. Uncertain disturbances are simulated by a white noise, and four sets of actuator fault signals, named as (a), (b), (c), (d) respectively, are set as (58)–(61). The

TABLE II
CONTROLLERS AND SMDO PARAMETERS

Parameter	Value	Parameter	Value	Parameter	Value
k_1	0.5	k_2	50	k_3	5
k_4	10	k_5	10	ρ_0	0.1 rad
l_1	50	l_2	1	ρ_∞	0.005 rad
σ	1	c	1	α_2	60
β_2	40	p_2	13	q_2	9
λ	60	μ	10	P_0	0.1 rad
P_{T_f}	0.0012 rad	T_f	1.5s	v	0.45
α_1	1	β_1	1	p_1	13
q_1	9	m	1	n	80;60(d)

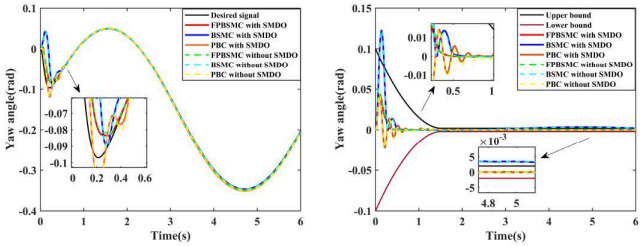

Fig. 8. Simulation results under fault (a). (a) Response curves to desired signal. (b) Tracking errors to desired signal.

parameters of observer and controllers are listed in Table II, where 60(d) denotes the value of this parameter is 60 when fault (d) occurs. The simulation results are shown in Figs. 8–12

$$(a):\begin{cases}\eta=1,\mathbf{T'}_e=0,0s\le t<0.3s\\ \eta=1,\mathbf{T'}_e=10000\sin(0.3t-2),0.3s\le t<1s\\ \eta=0.8,\mathbf{T'}_e=0,t\ge 1s\end{cases} \tag{58}$$

$$(b):\begin{cases}\eta=1,\mathbf{T'}_e=0,0s\le t<0.3s\\ \eta=1,\mathbf{T'}_e=30000\sin(0.3t-2),t\ge 0.3s\\ \eta=0.7,\mathbf{T'}_e=30000\sin(0.3t-2),t\ge 1s\end{cases} \tag{59}$$

$$(c):\begin{cases}\eta=1,\mathbf{T'}_e=0,0s\le t<0.3s\\ \eta=1,\mathbf{T'}_e=60000\sin(0.3t-2),t\ge 0.3s\\ \eta=0.4,\mathbf{T'}_e=60000\sin(0.3t-2),t\ge 1s\end{cases} \tag{60}$$

$$(d):\begin{cases}\eta=1,\mathbf{T'}_e=0,0s\le t<0.3s\\ \eta=1,\mathbf{T'}_e=100000\sin(0.3t-2),t\ge 0.3s\\ \eta=0.1,\mathbf{T'}_e=100000\sin(0.3t-2),t\ge 1s.\end{cases} \tag{61}$$

Obviously, it can be seen from Fig. 8(a) and (b) that FPBSMC has better control performance than BSMC and PBC. Especially, FPBSMC controller's error peak is smaller, the convergence rate is faster, and the final error is reduced and strictly limited within the prescribed boundary. Comparatively, the error of BSMC seriously exceeds the boundary. From Figs. 9–11, it can be seen that, as the aggravation of actuator faults, the performance of BSMC and PBC significantly deteriorates whether

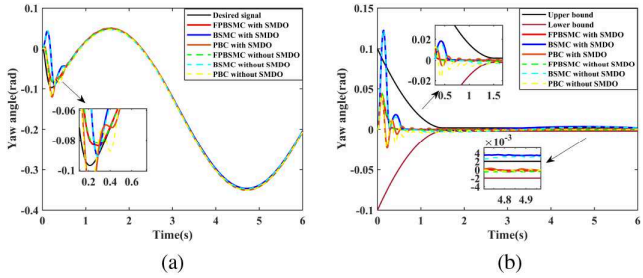

Fig. 9. Simulation results under fault (b). (a) Response curves to desired signal. (b) Tracking errors to desired signal.

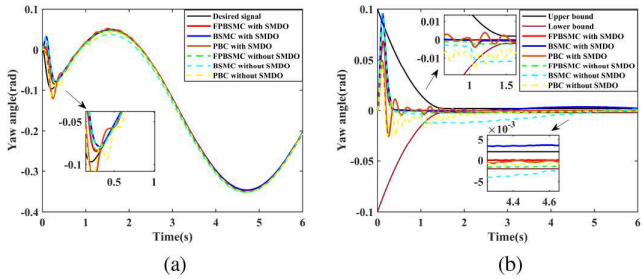

Fig. 10. Simulation results under fault (c). (a) Response curves to desired signal. (b) Tracking errors to desired signal.

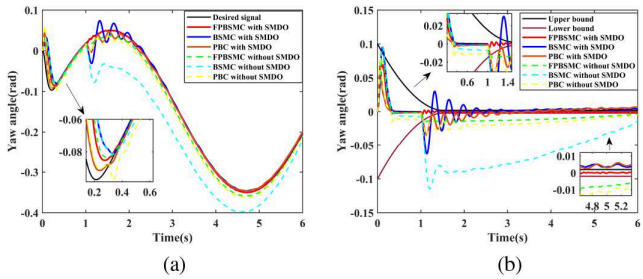

Fig. 11. Simulation results under fault (d). (a) Response curves to desired signal. (b) Tracking errors to desired signal.

SMDO is imposed or not. However, the performance of FPBSMC controller remains relatively stable. Furthermore, the introduction of SMDO helps reduce the tracking errors. Fig. 11(a) and (b) demonstrate BSMC and PBC fluctuate severely when fault occurs and fail to control PSC to track the desired attitude angle, with the error drastically exceeding the boundary. For the FPBSMC controller, although the error exceeds the boundary before SMDO is introduced, it still provides better control performance than BSMC and PBC. After introducing SMDO, FPBSMC can accurately track the desired signal, effectively keep the tracking error within the prescribed boundary, and show excellent fault tolerance performance. It can be seen from Fig. 12, SMDO accurately estimates the lumped disturbance torque caused by actuator faults and uncertain disturbances, significantly improving the fault tolerance of the controller through feedback compensation. The introduction of the observer not only enhances the tracking accuracy but also further reduces the steady-state error.

3) Complex Mission: The desired signal is set as a chirp signal with time-varying frequency and amplitude. The tracking performance of the chirp signal effectively validates the

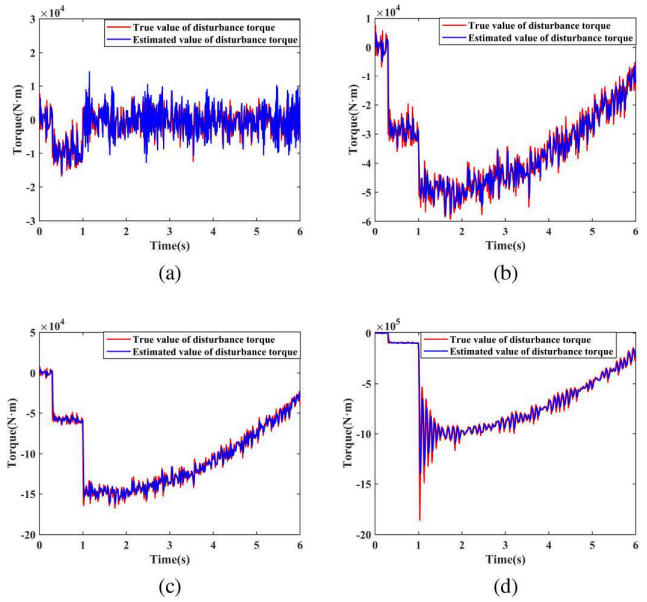

Fig. 12. Observer results. (a) Fault (a). (b) Fault (b). (c) Fault (c). (d) Fault (d).

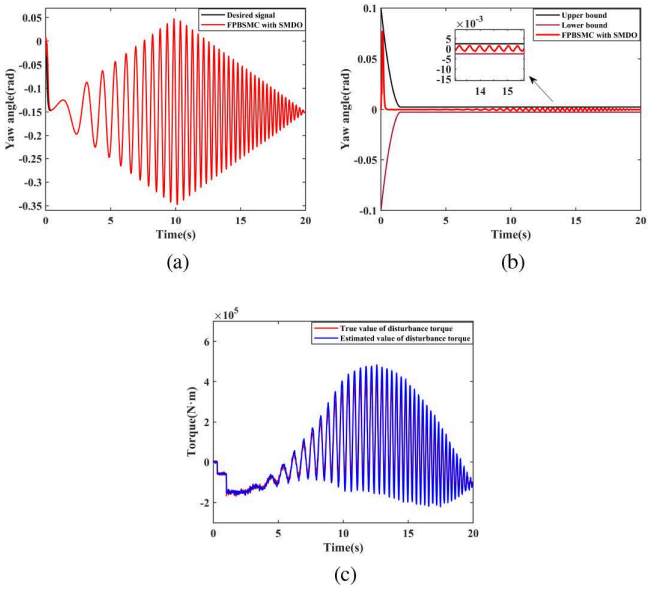

Fig. 13. Simulation results of chirp signal. (a) Response curve to desired signal. (b) Tracking error to desired signal. (c) Observer result.

robustness of the FPBSMC with SMDO control framework and its capability to handle complex tasks. The simulation results under fault (c) are shown in Fig. 13. As demonstrated in Fig. 13(a) and (b), the FPBSMC controller achieves high-precision tracking of the desired signal, with rapid convergence of the tracking error that remains strictly limited within the prescribed error boundaries. Furthermore, it can be seen from Fig. 13(c) that SMDO provides an accurate estimation of the lumped-disturbance torque, enabling effective compensation.

C. Hardware-in-Loop Experiment

In this part, we build a hardware-in-loop experimental platform, shown in Fig. 14, to further testify the practical

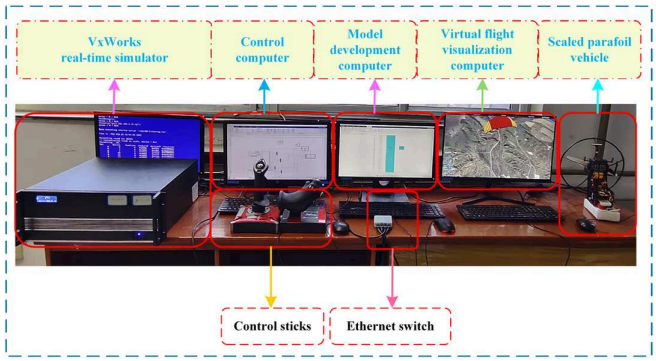

Fig. 14. Diagram of hardware-in-loop experimental platform.

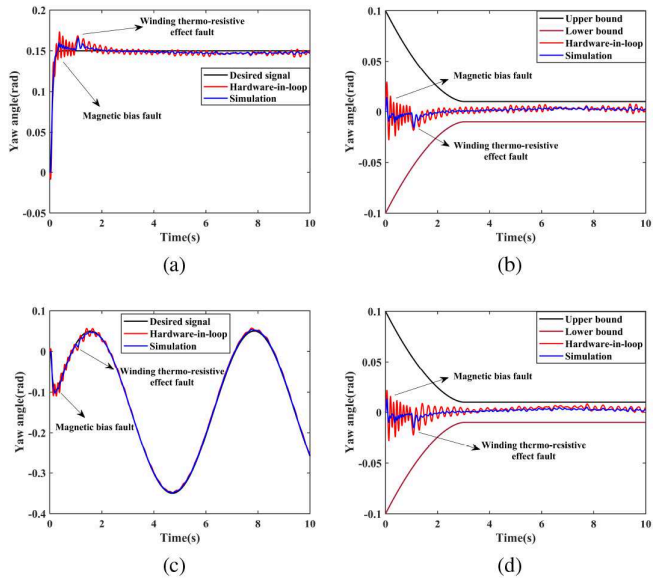

Fig. 15. Results of hardware-in-loop experiment. (a) Response curve to the step signal. (b) Tracking error to step signal. (c) Response curve to the sinusoidal signal. (d) Tracking error to sinusoidal signal.

application capability of FPBSMC with SMDO. The platform includes a real-time simulator (Links-Box-03, Beijing LinksTech Company, Ltd.) running VxWorks operating system combined with a model development computer, a control computer, a virtual flight visualization computer, control sticks, a scaled parafoil vehicle, and an ethernet switch. PSC model is deployed on the real-time simulator by the model development computer through the ethernet switch to ensure real-time calculation of experiment. The control computer runs FPBSMC in real time to control scaled parafoil vehicle automatically, or connect sticks to control scaled parafoil vehicle manually. The virtual flight visualization computer can display 3-D animations of the PSC trajectory and attitude. The scaled parafoil vehicle is equipped with actuators consisting of digital servos and operating levers. User datagram protocol (UDP) data communication between components of the platform is realized through the ethernet switch.

In hardware-in-loop experiment, FPBSMC with SMDO controls the scaled parafoil vehicle, and the fault c in (58) is simulatively introduced. The desired signals in the experiment are a sinusoidal signal and a step signal, which are identical to

Section IV-A and IV-B. The experimental results are illustrated in Fig. 15. It can be seen from Fig. 15(a) and (c) that FPBSMC can accurately control the PSC to track the desired signal. As shown in Fig. 15(b) and (d), the tracking error is constrained within the boundary and converges in finite time, which confirms the effectiveness of the proposed control strategy. However, there are still burrs and fluctuation in tracking and error curves, which can be attributed to the communication time delay inherent in the hardware experimental platform. Consequently, during the hardware-in-loop experiment, the controller parameters are adjusted with a relaxation of the boundary constraints to accommodate these practical implementation considerations.

V. Conclusion

First, the PSC actuator fault model is established in this article. Then, based on this model, FPBSMC attitude fault-tolerant controller combined with SMDO is designed, of which SMDO precisely and timely estimates the lumped disturbance torque caused by actuator faults and uncertain disturbances, thereby FPBSMC can effectively compensate for these disturbance torque's side-impact. By introducing PPC and combining with the BSMC, FPBSMC controller is proposed to improve both attitude tracking accuracy and fault tolerance performance, which ensures precise attitude control of the PSC during the recovery process. Finally, digital simulation and hardware-in-loop experiments are conducted to verify the feasibility of the proposed approach, which experimental results demonstrate that the proposed scheme effectively achieves fault-tolerant attitude control of PSC under actuator faults and uncertain disturbances. This research possesses substantial theoretical and practical significance in promoting reusable rocket technology and decreasing space launch costs. Future studies could concentrate on alleviating or eliminating the negative impacts of stochastic time delays on control performance and system stability.

References

[1] X. Xing, R. Wang, Q. Gong, and B. Xiao, "Terminal trajectory planning for the first-stage booster of rocket recovery by parafoil system in complex obstacle environments," *IEEE Trans. Aerosp. Electron. Syst.*, vol. 60, no. 4, pp. 4979–4993, Aug. 2024.

[2] M. Hashemi and C. P. Tan, "Integrated fault estimation and fault tolerant control for systems with generalized sector input nonlinearity," *Automatica*, vol. 119, 2020, Art. no. 109098.

[3] H. Teng, Y. Zhu, J. Qiao, X. Yao, and L. Guo, "Composite attitude tracking control for launch vehicles subject to actuator degradation fault and multiple disturbances," *IEEE Trans. Ind. Informat.*, vol. 20, no. 7, pp. 9275–9285, Jul. 2024.

[4] M. Van, M. Mavrovouniotis, and S. S. Ge, "An adaptive backstepping nonsingular fast terminal sliding mode control for robust fault tolerant control of robot manipulators," *IEEE Trans. Syst., Man, Cybern.: Syst.*, vol. 49, no. 7, pp. 1448–1458, Jul. 2019.

[5] S. Lian, Y. Zhu, W. Meng, K. Shao, and H. Li, "Adaptive fault-tolerant control for quadrotor based on the second-order fast nonsingular terminal sliding mode control," *IEEE Trans. Ind. Electron.*, vol. 72, no. 8, pp. 8322–8332, Aug. 2025.

[6] C. Liu, H. Chen, B. Jiang, Y. Zhang, and S. Xie, "Adaptive reconfigurable fault-tolerant control of multi-USVs with actuator magnitude and rate faults," *IEEE Trans. Ind. Electron.*, vol. 72, no. 8, pp. 8512–8521, Aug. 2025.

[7] W. Hao, B. Xian, and T. Xie, "Fault-tolerant position tracking control design for a tilt tri-rotor unmanned aerial vehicle," *IEEE Trans. Ind. Electron.*, vol. 69, no. 1, pp. 604–612, Jan. 2022.

[8] J. Gao, Z. Fu, and S. Zhang, "Adaptive fixed-time attitude tracking control for rigid spacecraft with actuator faults," *IEEE Trans. Ind. Electron.*, vol. 66, no. 9, pp. 7141–7149, Sep. 2019.

[9] Q. Shen, C. Yue, C. H. Goh, and D. Wang, "Active fault-tolerant control system design for spacecraft attitude maneuvers with actuator saturation and faults," *IEEE Trans. Ind. Electron.*, vol. 66, no. 5, pp. 3763–3772, May 2019.

[10] F. Jia and X. He, "Active fault-tolerant control with adaptive estimation error compensation for nonlinear systems: Achieving asymptotic tracking," *IEEE Trans. Ind. Informat.*, vol. 20, no. 4, pp. 6612–6621, Apr. 2024.

[11] H. Dong, Y. Zheng, X. Song, and S. Gao, "Reinforced safe performance cooperative control with event-triggered implementation for train formation," *IEEE Trans. Ind. Informat.*, vol. 20, no. 7, pp. 9588–9598, Jul. 2024.

[12] B. Xiao, H. Zhang, Z. Chen, and L. Cao, "Fixed-time fault-tolerant optimal attitude control of spacecraft with performance constraint via reinforcement learning," *IEEE Trans. Aerosp. Electron. Syst.*, vol. 59, no. 6, pp. 7715–7724, Dec. 2023.

[13] S. Yang, Y. Pan, L. Cao, and L. Chen, "Predefined-time fault-tolerant consensus tracking control for multi-UAV systems with prescribed performance and attitude constraints," *IEEE Trans. Aerosp. Electron. Syst.*, vol. 60, no. 4, pp. 4058–4072, Aug. 2024.

[14] H. Yu, Y. Ma, B. Jiang, and H. Ren, "An adaptive fault-tolerant control scheme for 6-dof spacecraft based on a control gain re-construction," *IEEE Trans. Aerosp. Electron. Syst.*, vol. 60, no. 4, pp. 5049–5059, Aug. 2024.

[15] M. Golestani, S. Mobayen, S. Ud Din, F. F. El-Sousy, M. T. Vu, and W. Assawinchaichote, "Prescribed performance attitude stabilization of a rigid body under physical limitations," *IEEE Trans. Aerosp. Electron. Syst.*, vol. 58, no. 5, pp. 4147–4155, Oct. 2022.

[16] S. Yin, B. Xiao, S. X. Ding, and D. Zhou, "A review on recent development of spacecraft attitude fault tolerant control system," *IEEE Trans. Ind. Electron.*, vol. 63, no. 5, pp. 3311–3320, May 2016.

[17] M. N. Hasan, M. Haris, and S. Qin, "Fault-tolerant spacecraft attitude control: A critical assessment," *Prog. Aerosp. Sci.*, vol. 130, 2022, Art. no. 100806.

[18] H. Sun, Q. Sun, M. Sun, J. Tao, and Z. Chen, "Accurate modeling and homing control for parafoil delivery system based on wind disturbance rejection," *IEEE Trans. Aerosp. Electron. Syst.*, vol. 58, no. 4, pp. 2916–2934, Aug. 2022.

[19] Y. Guo, J. Yan, C. Wu, and B. Xiao, "Modeling and practical fixed-time attitude tracking control of a paraglider recovery system," *ISA Trans.*, vol. 128, pp. 391–401, Sep. 2022.

[20] T. Song, L. Fang, Y. Zhang, and H. Shen, "Recursive terminal sliding mode based control of robot manipulators with a novel sliding mode disturbance observer," *Nonlinear Dyn.*, vol. 112, no. 2, pp. 1105–1121, 2024.

[21] K. Shao, J. Zheng, K. Huang, H. Wang, Z. Man, and M. Fu, "Finite-time control of a linear motor positioner using adaptive recursive terminal sliding mode," *IEEE Trans. Ind. Electron.*, vol. 67, no. 8, pp. 6659–6668, Aug. 2020.

[22] X. Bu, "Prescribed performance control approaches, applications and challenges: A comprehensive survey," *Asian J. Control*, vol. 25, no. 1, pp. 241–261, 2023.

[23] Z. Yin, A. Suleman, J. Luo, and C. Wei, "Appointed-time prescribed performance attitude tracking control via double performance functions," *Aerosp. Sci. Technol.*, vol. 93, 2019, Art. no. 105337.

[24] J. Han, "From PID to active disturbance rejection control," *IEEE Trans. Ind. Electron.*, vol. 56, no. 3, pp. 900–906, Mar. 2009.

Xiaojun Xing (Member, IEEE) received the B.S. degree in thermal engineering, and the M.S. and Ph.D. degrees in control theory and control engineering from the Northwestern Polytechnical University, Xi'an, China, in 1999, 2002, and 2008, respectively.

He is currently an Associate Professor with the School of Automation, Northwestern Polytechnical University. His research interests include fight control and guidance, navigation, and control of unmanned aerial/ground vehicles.

Wenxin Yang received the B.Eng. degree in automation in 2023 from the Northwestern Polytechnical University, Xi'an, China, where he is currently working toward the master's degree in control science and engineering.

His research interests include aircraft modeling and simulation, and fight control.

Linfeng Qin received the B.Eng. degree in automation from Changan University, Xi'an, China, in 2022, and the master's degree in electronic information from the Northwestern Polytechnical University, Xi'an, China, in 2025.

He is currently an Assistant Engineer with Xi'an ASN Technology Group Company Ltd., Xi'an, China. His research interests include aircraft modeling and simulation, and fight control.

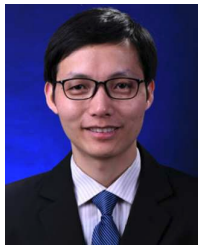

Bing Xiao (Senior Member, IEEE) received the B.S. degree in mathematics from Tianjin Polytechnic University, Tianjin, China, in 2007, and the M.S. and Ph.D. degrees in control science and engineering from Harbin Institute of Technology, Harbin, China, in 2010 and 2014, respectively.

He is currently a Professor with the School of Automation, Northwestern Polytechnical University, Xi'an, China. His research interests include aircraft control, advanced control design, and its application to unmanned aerial vehicles.

Feisheng Yang (Member, IEEE) received the Ph.D. degree in control theory and control engineering from Northeastern University, Shenyang, China, in 2013.

Since 2013, he has been an Associate Professor with Northwestern Polytechnical University (NPU), Xi'an, China. He is currently a Postdoctoral Supervisor with Northwestern Polytechnical University, Xi'an, China. His research interests include autonomous intelligent systems, new power systems, reinforcement learning and distributed optimisation, cybersecurity, and intelligent control.